



OPEN

Characterization of spent nuclear fuel canister surface roughness using surface replicating molds

B. L. Nation¹, J. L. Faubel², G.T. Vice³, J. A. Ohlhausen², S. Durbin³, C. R. Bryan¹ & A. W. Knight¹✉

In this study we present a replication method to determine surface roughness and to identify surface features when a sample cannot be directly analyzed by conventional techniques. As a demonstration, this method was applied to an unused spent nuclear fuel dry storage canister to determine variation across different surface features. In this study, an initial material down-selection was performed to determine the best molding agent and determined that non-modified Polytek PlatSil73-75 provided the most accurate representation of the surface while providing good usability. Other materials that were considered include Polygel Brush-On 35 polyurethane rubber (with and without Pol-ease 2300 release agent), Polytek PlatSil73-25 silicone rubber (with and without PlatThix thickening agent and Pol-ease 2300 release agent), and Express STD vinylpolysiloxane impression putty. The ability of PlatSil73-25 to create an accurate surface replica was evaluated by creating surface molds of several locations on surface roughness standards representing ISO grade surfaces N₃, N₅, N₇, and N₈. Overall, the molds were able to accurately reproduce the expected roughness average (R_a) values, but systematically over-estimated the peak-valley maximum roughness (R_z) values. Using a 3D printed sample cell, several locations across the stainless steel spent nuclear fuel canister were sampled to determine the surface roughness. These measurements provided information regarding variability in normal surface roughness across the canister as well as a detailed evaluation on specific surface features (e.g., welds, grind marks, etc.). The results of these measurements can support development of dry storage canister ageing management programs, as surface roughness is an important factor for surface dust deposition and accumulation. This method can be applied more broadly to different surfaces beyond stainless steel to provide rapid, accurate surface replications for analytical evaluation by profilometry.

In this study, we present a replication method to determine surface roughness and identify surface features when the sample cannot be directly analyzed by conventional techniques. As a demonstration, this method was applied to an empty full-scale spent nuclear fuel (SNF) dry storage canister to determine the surface roughness across different surface features. This method is intended only as a surface characterization method and not as an inspection method for in-service spent nuclear fuel canisters. This method has the flexibility to be used on a variety of complex surfaces; a spent nuclear fuel canister was selected as an exemplar due to the inability to measure the surface roughness directly using other methods.

Quantifying the surface roughness of natural and manufactured surfaces at the micron and sub-micron scales can provide critical information that spans many applications¹⁻⁴. These applications range from developing advanced engineered materials, to characterization of archeological specimens or biological samples (including teeth for dental applications)⁴⁻⁷. The ability to measure and quantify the surface roughness of a sample can provide details on material performance, susceptibility to degradation, and material interactions. Conventional direct measurement methods to determine surface roughness generally require the sample to be placed on a stage for analysis using atomic force microscopy (AFM) or profilometry in an analytical facility. Surface analysis techniques such as stylus or optical profilometry require expensive, highly sensitive equipment and are generally not feasible for use in field applications, especially when the surface of interest is outdoors. While these methods

¹Nuclear Energy Fuel Cycle Storage and Transportation Technology, Sandia National Laboratories, 1515 Eubank Blvd SE, Albuquerque, NM 87123, USA. ²Materials Characterization and Performance, Sandia National Laboratories, 1515 Eubank Blvd SE, Albuquerque, NM 87123, USA. ³Advanced Nuclear Fuel Cycle Technology, Sandia National Laboratories, 1515 Eubank Blvd SE, Albuquerque, NM 87123, USA. ✉email: aknight@perspectivetherapeutics.com

are highly sophisticated, sometimes the sample is such that surface roughness cannot be measured directly. For example, a sample may be too large for transportation to the analysis equipment or have a geometry that cannot be properly oriented in the system, the sample may not be suitable for measurement (e.g., too transparent or reflective for optical profilometry), or the sample may be prone to movement during the sampling (e.g., biological samples). One solution to the problem of sample incompatibility is to create a surface replica and analyze the replica using conventional direct measurement techniques^{1–11}.

Surface replication is a method of recreating a surface (or a negative of the surface) using a conformal mold with the intention of performing ex-situ topographical analysis when the sample cannot be analyzed directly. Surface replication for direct measurement is a technique that has spanned many applications and many different materials have been investigated^{1–13}. While the application of surface molds is becoming wide spread, few studies have attempted to quantify the accuracy of the mold to create a surface replica^{1,3,4,12}. One study found that differences in measured surface features were caused by differences in material color and transparency when analyzing by laser profilometry¹². Other studies directly compared different replicating materials. For example, a study by Goodall, et al.¹ investigated several different materials, including four different polyvinylsiloxanes (PVSs), two different room temperature vulcanizing rubber compounds, and one heat-accelerated vulcanizing rubber compound. The authors provided a statistical basis for replication accuracy and determined that President Jet light/regular body (low/medium viscosity) polyvinylsiloxanes provided the most accurate representations of the teeth and jaw samples analyzed, but noted these materials may be less effective on smooth or large surfaces (due to the fast cure time of 60 s).^{1,3} A subsequent study by Macdonald, et al.³ investigated the ability of four different polyvinylsiloxanes to accurately replicate the specific features on the surfaces of a *Dama Dama* pre-molar tooth, a penny, and a chert tool confirmed that these low and medium viscosity PVS cannot fully replicate complex micro-topologies. It was concluded by Macdonald, et al.³ that continued and ongoing investigations into different replicating materials would greatly facilitate more accurate understanding of surface features of specimens with complex topologies.

Here, we present the use of Polytek PlatSil 73–25 as a surface replication material following testing of several other materials and material additives. To date, there have been no studies investigating this material and its ability to accurately replicate a surface. In this study, the ability of the PlatSil 73–25 to reproduce a surface of known roughness was verified using surface roughness standards. Additionally, a 3D printed sample cell was created for this application to accommodate surfaces varying geometries and orientations for replication. Lastly, this study demonstrates the use of PlatSil 73–25 to effectively determine the surface roughness and variability in roughness of various surface features that occur on an empty full-scale SNF stainless steel (SS) dry storage canister. An SNF storage canister represents an ideal test specimen for this study because it is far too large for movement or direct profilometry measurements, but it has been shown that surface roughness may play a role in particulate deposition^{14–16} and pitting susceptibility^{17–19}. Therefore, understanding the variation in surface roughness across various features can provide information for canister aging management programs.

Results

Material Selection

Several materials were initially tested as possible molding materials to be used on an SS plate and an SNF canister to determine the surface roughness.¹⁹ Initial testing evaluated both usability of the material and the ability of the material to replicate the surface. These materials were Polygel Brush-On 35 polyurethane rubber, Polytek PlatSil73-25 silicone rubber, and Express STD vinylpolysiloxane impression putty. The Polygel Brush-On 35 polyurethane rubber and Polytek PlatSil73-25 were evaluated with and without Pol-ease 2300 release agent. Also, the Polytek PlatSil73-25 was evaluated with and without the PlatThix thickening agent. The Polygel Brush-On 35 Rubber was not effective for this application because it was applied by brushing onto the surface and the resulting mold did not successfully replicate the surface—therefore, it was eliminated from further testing. The Express STD vinylpolysiloxane impression putty cured quickly but had an extremely high viscosity which made it difficult to apply to the candidate surface, so it was eliminated from further testing. PlatSil73-25 is a 2-part silicone that, when mixed, forms a viscous fluid that can be poured into a retaining structure on the metal surface. After curing (> 5 h), PlatSil73-25 was easy to remove from the surface and a release agent was determined to be unnecessary. Experiments were carried out to determine the impact of the PlatThix thickening agent on the PlatSil73-25. These tests demonstrated that the more thickening agent used, the softer the resulting cured silicone rubber. Also, the addition of PlatThix resulted in bubbles in the resulting surface mold, and the number of bubbles increased with the volume percent of the thickening agent added. Overall, PlatSil 73–25 performed best when no thickening agent or release agent was added.

Verification of the effectiveness of PlatSil73-25 with surface roughness standard

The ability of PlatSil 73–25 silicone rubber to replicate a surface was verified using a surface roughness standard (SPI Microsurf 326 (Linishing) and SPI Microsurf 315 (Surface Grinding)) collected in a horizontal configuration. Each standard had six regions, each with a different surface roughness corresponding to an ISO surface roughness of N₃–N₈ (Linishing and Grinding) The six regions featured directional polishing grooves; therefore, the roughness was measured perpendicular to the grooves. Two test areas on each standard were replicated with the PlatSil73-25. The confocal measurement was performed using a 658 nm laser using a 20× objective resulting in a Z-resolution of 5 nm and spatial resolution of 230 nm. Roughness was determined via a line analysis at several transects across the grooves. PlatSil 73–25 was applied across sections of the standard corresponding to N₃ (R_a = 0.10 μm; R_z = 0.90 μm), N₅ (R_a = 0.4 μm; R_z = 2.60 μm), N₇ (R_a = 1.60 μm; R_z = 18.5 μm), and N₈ (R_a = 3.2 μm; R_z = 15.6 μm) (Fig. 1), and all the standards surfaces were measured directly and compared with the replicating molds.

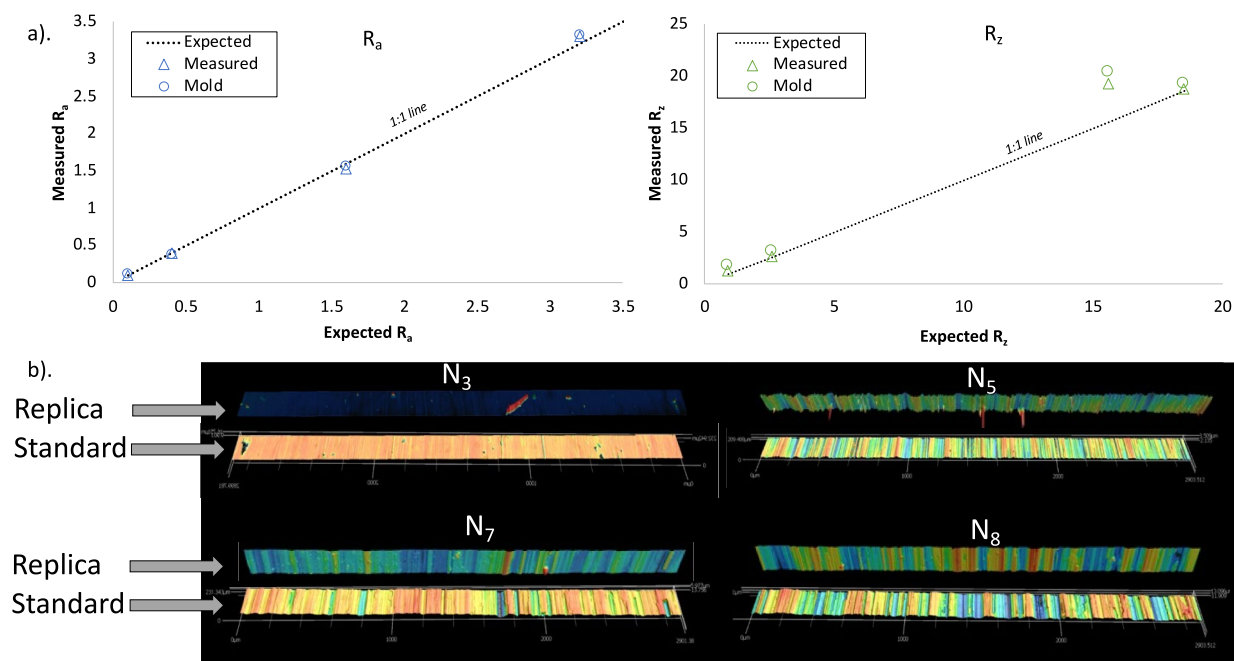


Fig. 1. (a). Measured surface roughness for the mold samples versus the measured surface roughness standard shown with a 1:1 line for R_a and R_z . (b) 3-D topographic maps of the surface roughness standards and the corresponding replica. Slight offsets in the images are due to small differences in the image size.

The surface roughness standard was measured directly at the N_3 , N_5 , N_7 , and N_8 locations as a calibration check of the confocal microscope. The measured R_a values were systematically higher than the roughness value listed on the standard and are shown in Table 1. Validation plots for R_a and R_z showing the direct measured roughness and mold roughness compared to the expected roughness are shown in Fig. 1a. Overall, the directly measured surface roughness corresponds well with the expected values on the surface roughness standard with an average error across all surfaces of 2.6%. Similarly, the mold generally produced a surface that matched the expected R_a with an average error of 7%. This was largely driven by the 21% error seen in the N_3 location. PlatSil 73–25 was able to replicate a rougher surface more accurately, probably due to the high viscosity of the polymer (~6000 cp–like molasses) which may prevent penetration of the epoxy into the smaller surface features, especially those with high aspect ratios. For the rougher test areas (N_8) the long-range waviness (λ_c) was not removed. The R_z value for the direct measurement corresponds well with the expected R_z on all cases except for the N_8 surface, where the expected value was 15.600 μm and the measured value was 19.243 μm . The mold produced R_z values that were systematically higher than the measured and expected values. Interestingly, the N_8 surface mold more closely resembled the measured value than the expected value, it is unclear why both deviated from the expected value. Overall, the excellent agreement between the replicating mold and the directly measured surface roughness standard can be seen visually in the 3D topographic map in Fig. 1b, where the molded surface is seen on top and the surface roughness standard is on bottom for N_3 , N_5 , N_7 , and N_8 .

ISO Grade	R_a (μm)			R_z (μm)		
	Expected	Measured	Mold Measured (Error ^b)	Expected	Measured	Mold Measured (Error ^b)
N_3 (Lining)	0.100	0.102	0.121 (– 0.19)	0.900	1.228	1.699 (– 0.38)
N_5 (Grinding)	0.400	0.406	0.394 (0.03)	2.600	2.569	3.128 (– 0.22)
N_7 (Lining)	1.600	1.545	1.578 (– 0.02)	18.500	18.773 ^a	19.185 ^a (– 0.02)
N_8 (Grinding)	3.200	3.310 ^a	3.342 ^a (– 0.01)	15.600	19.243 ^a	20.359 ^a (– 0.06)

Table 1. Expected surface roughness values shown with the directly measured surface and measure mold values for N_3 , N_5 , N_7 , and N_8 . Replication error is shown in parentheses. ^aLong range waviness λ_c was not removed. ^bError calculation: (Measured – Mold Measured) / Measured.

Test application: stainless steel spent nuclear fuel dry storage canister

To date, much of the work done in creating surface replicating molds has focused on archeological or biological (e.g., teeth) specimens. The roughness of a SNF dry storage canister has not previously been characterized due to its large size. The canister surveyed was NUHOMS 32 PWR Canister. Canister locations were chosen to represent the range of surface features present, to capture the representative mill finish canister surface, ground weld regions, the weld-adjacent heat affected zones (HAZ), and any other regions that showed evidence of grinding or alteration during manufacturing. The canister surface mill finish was expected to fall within the range of the surface roughness standards—from $0.1 \mu\text{m} < R_a < 3.2 \mu\text{m}$ and $0.90 \mu\text{m} < R_z < 18.5 \mu\text{m}$. Locations of surface features (e.g. grinding marks, welds, etc.) on the canister were marked and the radial and lateral coordinates were determined.²⁰

The canister was oriented in a horizontal configuration and radially aligned by a drain hole in the grappling ring at the bottom. Specific alignment details can be seen in Knight, et al.²¹ and visualized in Fig. 2. When the drain hole is aligned vertically (top and bottom), the canister is in its standard orientation. In this orientation, the longitudinal welds are at $\sim 140^\circ$ and 320° radial positions (when looking at the grappling ring) and extend the full length of the canister until intersected by circumferential welds at each end. The orientation of the coordinate system is shown in Fig. 2a, where the longitudinal origin is at the open end of the canister (where the SNF is loaded) and increases toward the grappling ring and the axial origin is the center of the topside and increases in a clockwise direction.

Examples of the surface features replicated in this study are shown in Fig. 2b and Fig. 2c. Regions investigated include welds, the weld adjacent HAZs regions, and mechanically altered regions. The mechanically altered regions investigated include i) large post-manufacturing bands (~ 6 inches to 1 foot wide) extending several feet circumferentially around the canister, ii) specific areas (a few square inches) that have been spot-ground, and iii) circumferential regions near the top and bottom of the canister that have undergone additional alterations.

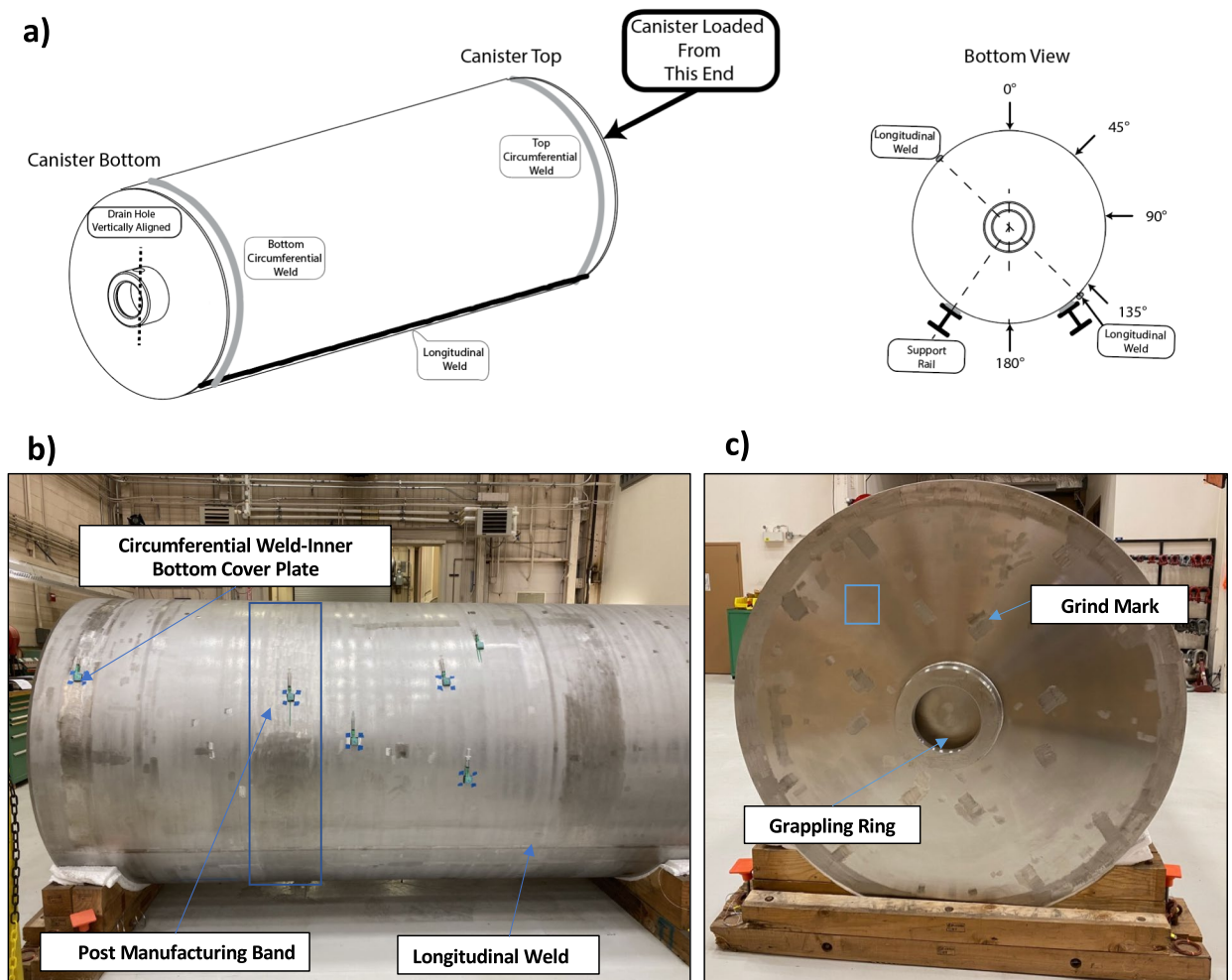


Fig. 2. NUHOMS 32PTH2 Canister; (a) schematic of canister in standard orientation with features of interest including longitudinal and circumferential welds and grappling ring; (b) side view of the canister to point out the longitudinal weld, the circumferential weld (Inner Bottom Cover Plate), as well as normal surface regions and the post manufacturing bands²². (c) Photo of the bottom of the canister showing the grappling ring, bottom surface, and grind marks.

The sample number and the surface feature they were used to sample are presented in Table 2 along with the corresponding measured R_a and R_z values of the surface replicating mold. For each region, the surface mold replicate was taken using the sampling cell and PlatSil73-25.

Normal surface roughness

Six locations on the canister were chosen to evaluate the mill finish and to evaluate the variability of the normal surface roughness across the canister (Samples 1–6). The locations were chosen to avoid any abnormal surface features such as grinding marks or welding bands. Figure 3 shows the canister sample images of the mold in-situ and optical image, and the 3D profile of the surface. From the images in Fig. 3 and the surface roughness values from Table 2 for Samples 1–6, it is clear that the mill finish across the canister is relatively uniform, where the average $R_a = 0.79 \pm 0.04 \mu\text{m}$ and $R_z = 4.19 \pm 0.3 \mu\text{m}$. There does not appear to be any directionality, as horizontal and vertical line scans resulted in similar surface roughness values. This surface roughness corresponds to about a 180-grit surface ($R_a = 0.76 \mu\text{m}^{23}$). Also, these values fall within the range of the roughness standards. Long range waviness was removed from all these samples, consistent with the calibration test.

Two samples were collected from the bottom of the canister near the grappling ring. The bottom of the canister is different from the rest of the canister surface as it has fine, uniform grooves likely from machining. Like the normal surface, the bottom of the canister had several randomly distributed grind marks. One sample, Sample 17, was collected to be representative of the bottom surface, and Sample 16 was taken from a grind mark on the bottom surface of the canister. The normal bottom surface topography (Sample 17) was uniform with small surficial grooves that run parallel to larger grooves at a uniform interval, about every $250 \mu\text{m}$ (Fig. 3). The reported R_a and R_z values did not use a λ_c filter because the filter removed the long-range features of the surface. Again, this treatment of the λ_c filter is consistent with the calibration test. The overall surface on the bottom of the canister was much rougher than the normal surface roughness seen on most of the canister and had an $R_a = 2.66 \mu\text{m}$ and $R_z = 11.34 \mu\text{m}$ and corresponds to a < 80 -grit surface.

Post-manufacturing band

Apart from the normal surface, the next most common surface features on the canister were large circumferential bands that occurred periodically, as seen in Fig. 3. These regions were visually distinct from the normal surface and possibly attributed to direct contact with the rollers when the canister was manufactured. One sample (Sample 12) was collected from one of these bands to evaluate the deviation in the surface roughness compared to the normal canister roughness. The sample results are shown in Fig. 3 and Table 2. Visually, these features resemble the topology of the normal surface, however the features appear to be muted (Fig. 3). The R_a and R_z values of this surface feature were smaller than those for the normal surface – thus representing a smoother surface. The R_a value was determined to be $0.53 \pm 0.01 \mu\text{m}$ and the R_z was determined to be $2.54 \pm 0.4 \mu\text{m}$. Based on the measured R_a value, this surface is slightly rougher than a 220-grit finish.

Weld regions and less common features

Welds and the weld-adjacent HAZs are of great interest on an SNF canister, as these regions are likely to contain high weld-related tensile stresses and hence are likely to be the most susceptible locations for chloride induced stress corrosion cracking (CISCC). For this discussion, the weld adjacent HAZ refers to the unground area

Sample #	Canister feature	R_a (μm)	R_z (μm)	Analysis scan orientation
1	Normal Surface (mill finish)	0.78	4.27	Vertical
2	Normal Surface (mill finish)	0.78	4.33	Vertical
3	Normal Surface (mill finish)	0.84	4.40	Vertical
4	Normal Surface (mill finish)	0.84	4.51	Horizontal
5	Normal Surface (mill finish)	0.76	3.88	Horizontal
6	Normal Surface (mill finish)	0.75	3.75	Vertical
7	Circum. Weld (Inner Bottom Cover Plate)	0.52	2.65	Vertical
8	Circum. Weld (Inner Bottom Cover Plate)	0.53	3.00	Vertical
9	Longitudinal Weld	1.41	1.86	Vertical
10	Longitudinal Weld	1.05	1.54	Vertical
11	Longitudinal Weld	0.81	1.58	Vertical
12	Post Manufacturing Band	0.53	2.54	Vertical
13	Grinding near with Support Ring Inner Circum. Weld	1.30	2.34	Vertical
14	Grind Mark	0.80	2.36	Vertical
15	Grind Mark	1.08	3.43	Vertical
16	Canister bottom – Grind Mark	0.61	3.14	Horizontal
17	Canister bottom (λ_c filter was not applied)	2.66	11.34	Horizontal

Table 2. Sample number, canister feature, approximate canister location, measured surface roughness (R_a and R_z), and scan direction for each surface mold collected from the canister.

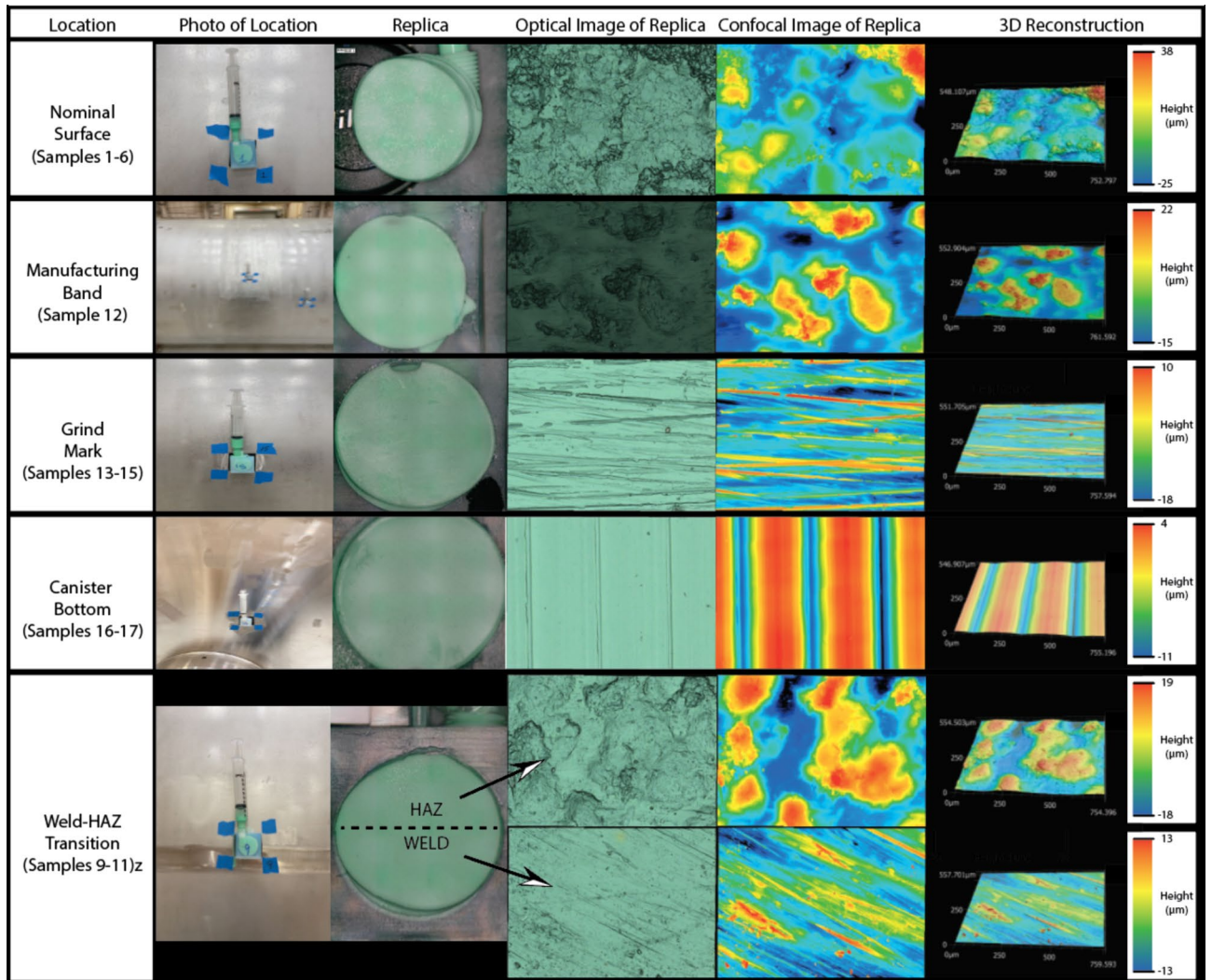


Fig. 3. Examples of the mounted surface mold, optical image of the surface mold, and a 3-D topographic map of the surface obtained by laser profilometry analysis demonstrating different features on the canister surface. The scales bars apply to both the 2D and 3D confocal images.

adjacent to the ground weld. When the SNF canister welds were manufactured they were ground flush to the surface; therefore, there is no clear weld toe and the boundary between the weld and the HAZ is not distinct. The likely width of the HAZ is 1–2 cm,²⁴ so some amount of the HAZ extends outside of the relatively narrow ground area of the weld on either side of the weld. Two longitudinal welds 180° apart span the entire length of the canister and are visible in b. There were also circumferential features associated with welds at the top and bottom of the canister. The circumferential band at the top of the canister is the external HAZ associated with the internal weld used to mount the inner support ring and was about the same width as the longitudinal weld. The circumferential weld at the bottom of the canister was ~5–7.5 cm (2–3 inches) wider than the longitudinal weld and visually appeared to have much more surface variation in the HAZ than in the weld region.

Two samples were collected from the circumferential weld at the bottom of the canister (Sample 7–8). Like the longitudinal welds, the circumferential welds were ground to remove the surface weld beads. In contrast to the circumferential feature represented by Sample 13, the surface features observed in the bottom circumferential weld were visibly larger and smoother when looking at the canister surface. The surface roughness of Samples 7 and 8 more closely resembled the large, post-manufacturing band, but had the directionality of the welded regions. The measured roughness of this canister feature was $R_a = 0.52 \pm 0.01 \mu\text{m}$ and $R_z = 2.82 \pm 0.2 \mu\text{m}$ corresponding to a 220-grit surface finish. Relative to the longitudinal welds, there is much less variability in the R_a and R_z values as well as smaller R_a values overall.

Three samples were collected from the longitudinal welds (Samples 9–11); Samples 9 and 10 were bisected by the weld and therefore also included the unground weld adjacent HAZ regions (Fig. 3). The differences between the weld region and the weld-adjacent HAZ region can be observed visually on the surface mold and in the 3-D maps. From the 3-D topographic maps of the welded regions, they appeared to exhibit some directionality in which fine surface features were parallel to the weld direction. This is due to grinding of the weld beads after welding. The profilometry scan direction was analyzed perpendicular to the directionality to account for this directionality. 3-D topographic maps collected from the HAZ regions resemble the mill finish, and do not appear

to have any clear directionality. This was expected since the weld adjacent HAZ regions are typically not ground after welding. The average surface roughness values for the longitudinal weld regions were $R_a = 1.09 \pm 0.3 \mu\text{m}$ and $R_z = 1.66 \pm 0.2 \mu\text{m}$. These regions had a higher R_a value than the normal surface but a lower R_z value. This suggests the roughness of the weld in terms of surface variability is greater than the normal surface, consistent with the visible grind marks; however, the depth of the features observed was generally smaller. The variation was much more substantial than seen for the normal surface. Samples 9, 10, and 11 were placed very close to each other in the longitudinal direction along the weld. However, the surface roughness varied a bit across the samples, Sample 9 had an $R_a = 1.41 \mu\text{m}$ and Sample 11 had an $R_a = 0.81 \mu\text{m}$. The weld regions on average corresponded with a grit of ~ 150 , however the corresponding grits for this large R_a range for the welds varies from about 120-grit to 180-grit. This variability was likely caused by the highly subjective and variable nature of hand-grinding. The associated images of the HAZ regions, which are the unground regions adjacent to the welds, were evaluated by analyzing the top section of Samples 9 and 10, are shown in Fig. 3. There was no clear directionality of the HAZ region, and topographically, the HAZ regions resemble the normal surface, and have a similar R_z value, though the R_a value is very different. The average HAZ roughness is $R_a = 3.11 \pm 0.2 \mu\text{m}$ and the is $R_z = 3.24 \pm 0.1 \mu\text{m}$. Due to the large R_a , the HAZ regions resemble a surface finish of 60 – 80 grits.

One sample was collected from the intersection of the longitudinal weld and the external weld adjacent HAZ region resulting from the circumferential weld at the top of the canister (Sample 13). The external surface appears to have been ground spanning the entire circumference. In addition, a few small pits were visually observed and evaluated by profilometry. The topographic map of this sample showed directionality parallel to the weld direction. The measured R_a was $1.30 \pm 0.2 \mu\text{m}$ and R_z was $2.33 \pm 0.5 \mu\text{m}$. This surface roughness was very similar to Sample 9, which was the roughest of the longitudinal weld samples and corresponded to a surface roughness of about 120-grit. This region was not as rough as the HAZ associated with the longitudinal welds; however, the R_a was much higher than other regions that had been ground.

Scattered across the canister were small regions that had been ground (seen in Fig. 2b,c). It is unclear why these regions were ground, however there are many of them across the canister surface. These grind regions may have been performed post manufacturing to remove specific flaws. Two locations were chosen to evaluate the surface roughness of these ground regions (Samples 14–15). The grind marks were visually distinct features on the canister and both samples had visible pits in the sampled region. The 3-D topographic maps of the surface resemble other features that have been further altered beyond the normal surface topography. There is clear directionality in the orientation of the surface features that align parallel to the canister direction, like the welds. The average R_a was $0.94 \pm 0.2 \mu\text{m}$ and R_z was $2.90 \pm 0.76 \mu\text{m}$. There was a decent amount of variability between the two samples and the roughness spanned comparable grinding roughness of 150–180 grit.

Figure 4 shows all the measured surface features and their respective R_a and R_z values. For unground areas like the normal surface and machined features the R_z was approximately 4 times higher than the R_a indicating that the peaks and valleys on the surface are much deeper than the average surface. Overall, individual measurements

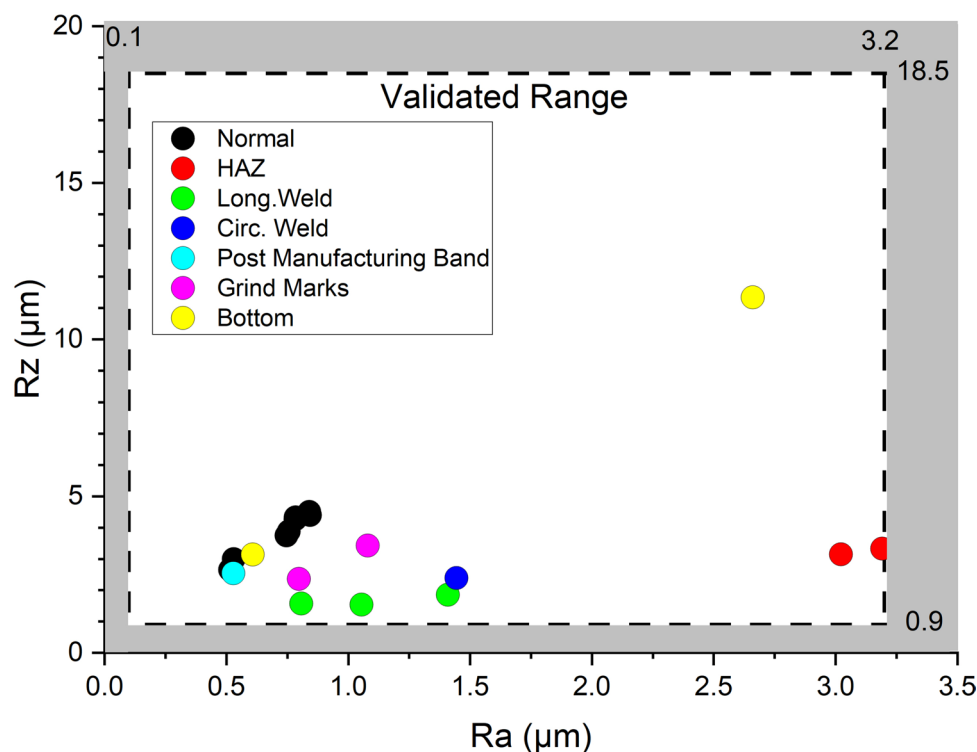


Fig. 4. R_z versus R_a for each of the replicas on different surface features. The grey area denotes the bounds of the region that was validated using the roughness standards.

on each type of surface were grouped tightly (with exception of the canister bottom surface) indicating a high amount of consistency in the topography of the surface across the canister. All measurements also fell within the bounds validated using the surface roughness standards, which provides a high degree of confidence that the replicated surface measurements are representative of the physical surface.

Surface anomalies

Mechanically-induced surface pits were observed on the canister surface co-located with three samples (Sample 13–15) and are shown in Fig. 5. These pits did not form by corrosion but rather are due to some mechanical process (gouges), or formed during welding (weld voids). In total, 20 pits were identified and analysis via profilometry of these pits was performed to assess their size and aspect ratio. The pits were generally hemispherical or semi-hemispherical with significant variability in the pit depth and width. The pits were shallow, as the average pit depth was $31.63 \pm 19.8 \mu\text{m}$, and the deepest measured pit was $85.67 \mu\text{m}$ (Sample 14). The pit width was generally much larger and more variable than the depth and often more than hundreds of microns wide, ranging from $48.15 \mu\text{m}$ (Sample 14) to $1878 \mu\text{m}$ (Sample 15). Figure 5 shows the distribution of pit width and depth of all the measured pits associated with Samples 13–15. The average aspect ratio was calculated (excluding the two outliers from Sample 14 with an aspect ratio near 1) as $[\text{Pit Depth}/\text{Pit Width}]$ and was plotted on the pit width versus pit depth graph. Overall, the average aspect ratio of the pits was 0.04 ± 0.02 , which represents a very shallow wide pit. The cumulative probability plot of the aspect ratio (Fig. 5c) shows that most of the pits $> 90\%$ had an aspect ratio < 0.1 .

The goal of evaluating these anomalous canister surface features is to assess the ability of the mold to capture complex geometries and allow for in-depth characterization. The ability to characterize minuscule surface features creates a tool for surface evaluation and a guide for surface replication. Macdonald, et al.³ evaluated the effectiveness of Coltene Affinis[®] (light and heavy body) and Heraeus Kulzer Provil[®] novo (light and medium body) to replicate the surface features of a penny and determined that all four measurements produced roughness that overestimated the size of the feature. While it is not possible to directly measure the size and shape of the pits evaluated on the canister surface, based upon their size and the calibration data, it is likely that the mold represents the size of the feature well. However, more work would be needed to statically inform this claim.

Discussion and conclusions

Quantifying the ability of a surface replicating mold to accurately mold a surface can enable its use for a variety of applications. After evaluation of several different materials, including Polygel Brush-On 35 polyurethane rubber, Polytek PlatSil73-25 silicone rubber (with and without PlatThix), and Express STD vinylpolysiloxane

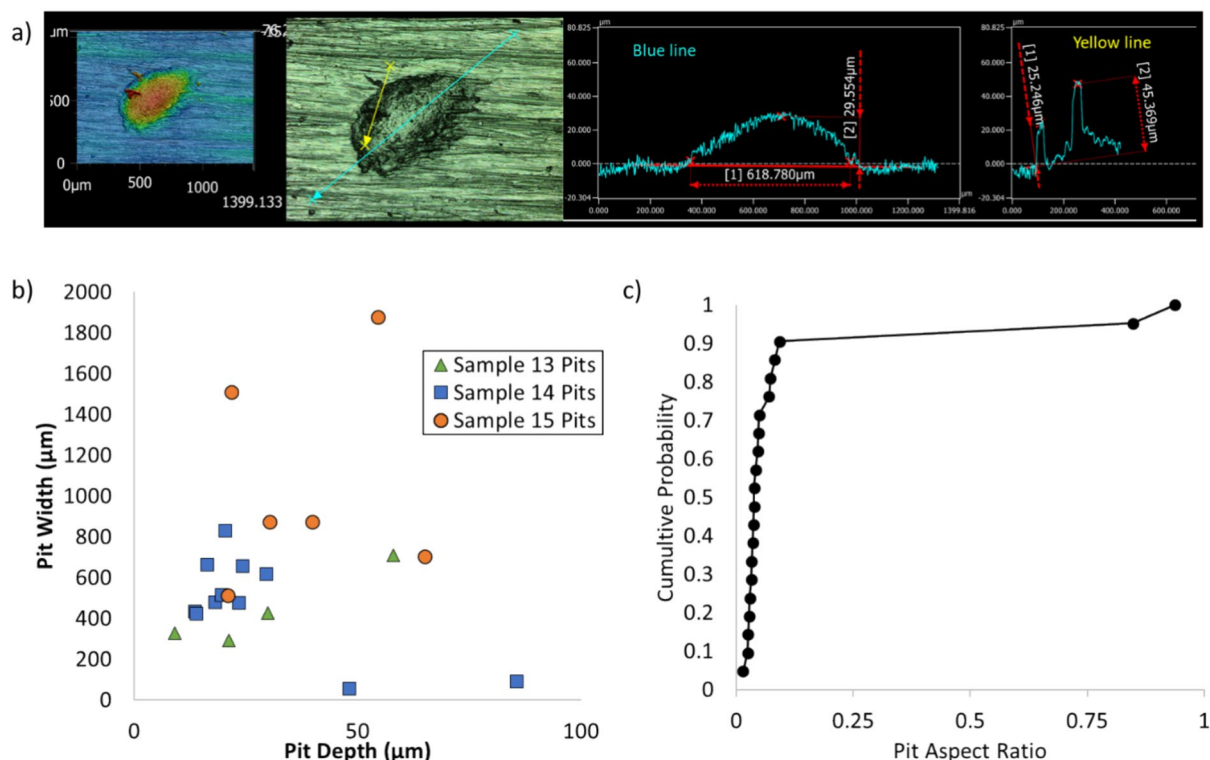


Fig. 5. (a) Pit analysis of a pit from Sample 14. The main pit is semi-hemispherical, shallow, and wide. This pit displays a small crack-like feature extending out from the rim of the pit. (b) The pit width versus pit depth shown with the average and standard deviation of the pit aspect ratio (excluding the two outliers with a high aspect ratio) shown with the standard deviation (σ), and (c) Cumulative probability versus aspect ratio of the mechanical pits identified.

impression putty, the Polytek PlatSil73-25 (without PlatThix) was selected for further evaluation due to its ability to replicate the surface, lack of bubbles, and its ease of use for complex sample geometries. The ability of Polytek PlatSil73-25 to accurately replicate a surface was demonstrated for the range of $R_a = 0.1 \mu\text{m}$ to $3.2 \mu\text{m}$ and $R_z = 0.9 \mu\text{m}$ to $18.5 \mu\text{m}$ using surface roughness standards with surfaces corresponding to ISO grades N_3 , N_5 , N_7 , and N_8 . Overall, the mold roughness, R_a , agreed well with the expected surface roughness but the R_z value systematically overestimated. This overestimation may be due to differences in reflectivity between the standard (metallic) and the replica (polymeric) as well as asymmetry in the surface feature distributions, such as when valleys on the standard become peaks in the replica and vice versa. The molding material was able to accurately capture the magnitude and location of the peaks and valleys in the surface standards despite a small systematic offset. For the standards, the R_z of the N_8 surface, measured directly and measured off the surface replicating mold, deviated the most from the expected value likely due to error in the surface standard that was used. To the best of our knowledge, this report is the first study evaluating the ability of PlatSil73-25 to accurately mold a surface and to perform a mold calibration with surface roughness standards.

Polytek PlatSil73-25 was applied to determine the surface roughness of a full scale SNF canister (NUHOMS 32PTH2-S023-C-H-001) to better understand the variation in normal surface roughness as well as provide an understanding of the differences in surface roughness of specific canister features (welds, grind marks, etc.). While there is no way to directly evaluate the canister surface to verify the accuracy of the molds, because the measured surface roughness falls within the calibrated range, we have confidence that the measure mold R_a values are accurate, and the measured mold R_z may slightly overestimate the actual R_z . The surface roughness of the normal, mill finish canister surface was $R_a = 0.79 \pm 0.04 \mu\text{m}$ and $R_z = 4.19 \pm 0.3 \mu\text{m}$ and corresponded to approximately a 180-grit finish. Features on the canister surface produced some variability in the surface roughness. For example, the weld areas were ground, and the measured surface mold roughness corresponded to an $R_a = 1.09 \pm 0.3 \mu\text{m}$ and $R_z = 1.66 \pm 0.2 \mu\text{m}$. A large post-manufacturing band was also evaluated, and the resulting mold has an $R_a = 0.53 \pm 0.01 \mu\text{m}$ and $R_z = 2.54 \pm 0.4 \mu\text{m}$, which was smoother than the normal canister surface. A subset of samples collected from grind marks on the canister surface showed that these grind marks were treated in a similar way to the welds — though not as extensively—and produced an R_a was $0.94 \pm 0.2 \mu\text{m}$ and R_z was $2.90 \pm 0.76 \mu\text{m}$. In addition to the roughness of the surface, specific anomalous surface features (i.e., mechanical pits) were evaluated and their size and shape was quantified.

This exercise has produced the first detailed analysis of the surface roughness of a full scale SNF canister. This may have implications on dust deposition for in-service canisters. This method will allow for an in-field determination of the surface roughness of parts that cannot be sent directly to a laboratory facility for direct measurement.

Additional studies using PlatSil73-25 on other types of samples should be performed to compare against other mold materials that have demonstrated success through a rigorous statistical evaluation. The useability of the PlatSil73-25 may enable its use for a variety of different sample types and geometries on metals surfaces. To date, no studies have been performed on ceramic, polymeric, or other types of surfaces, though it is likely the mold will create a functional surface replicate.

Methods

Surface replicating materials

Three different materials were evaluated for this study, Polygel Brush-On 35 polyurethane rubber, Polytek PlatSil73-25 silicone rubber, and Express STD vinylpolysiloxane impression putty. Modifications were explored for the Polygel Brush-On35 and the PlatSil73-25. Specifically, the Polygel Brush-On 35 polyurethane rubber and Polytek PlatSil73-25 were evaluated with and without Pol-ease 2300 release agent. In addition, the Polytek PlatSil73-25 was evaluated with and without the PlatThix thickening agent. All materials were mixed following the manufacturer specifications.

Sample cell and surface sampling

A sample cell was designed so that the molding material could cure on a surface in any location and orientation¹⁹. This sample cell was designed to adhere to a surface using an adhesive gasket and then be injected with the molding material in situ. Based on the surface features of interest for this sampling technique, the sample cell window was created to be 25.4 mm (1 inch) in diameter. This small size meant it could be analyzed using most lab-scale profilometry methods (stylus, optical, etc.). A drawing of the sample cell is shown in Fig. 6a and example sample cell in Fig. 6b.

The surface replication technique used followed a simple procedure to create a negative replica of a surface to be analyzed by laser profilometry. To achieve the sample mold, first, an adhesive gasket was used to adhere to sampler to the specimen surface. Next, the Polytek PlatSil73-25 silicone rubber was mixed in a 1:1 ratio per vendor instructions and the mixed contents were transferred to a 10 mL syringe. The syringe was directly connected to the sample cell inlet via Luer lock fitting, and the silicone rubber was injected into the sample cell until it filled the sample cell and a small amount escaped through the air vent to ensure that the cell was filled. The sample cell, filled with the surface replicating material, was allowed to cure (~24 h). Once cured, the adhesive gasket and sample cell were carefully peeled off the surface and the solidified silicone rubber puck with a negative replica of the surface (Fig. 6c) was analyzed by profilometry.

Profilometry

The surface roughness of the material in the sample window was evaluated using a Keyence VK-X150 laser scanning confocal microscope. For each sample, a stitched image was acquired using a $50\times$ standard working distance (WD) objective to create analysis regions of $\sim 550 \mu\text{m} \times 755 \mu\text{m}$ for molded samples or $3000 \mu\text{m} \times 200 \mu\text{m}$

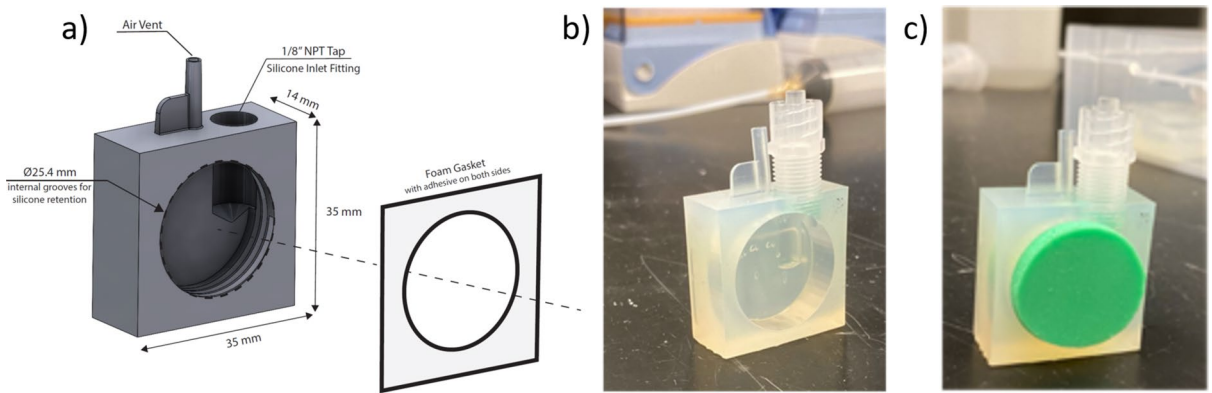


Fig. 6. (a) Rendering of the surface replicator cell with adhesive foam gasket with the sampling cell is shown empty (b) and with PlatSil 73–25 silicone rubber (c) following 24 h of curing on a SS surface.

for unidirectional surface roughness standards. To determine the size of larger/anomalous features (e.g., pits), a $10\times$ standard WD objective was used. Images were plane leveled, and a medium height cut was applied prior to analysis for noise reduction. An average of 11-line profiles were collected across the image in both directions and reported surface roughness was from the direction where the roughness was highest, and the standard deviation was lowest.

The line scans were averaged to determine the R_a and R_z for each sample. R_a represents the arithmetic mean of the absolute surface roughness^{25,26}, calculated by:

$$R_a = \frac{1}{l} \int_0^l |z(x)| dx \quad (1)$$

where l is the length of the line scan, and $|z(x)|$ is the absolute value of the surface topography as a function of position in the x direction. R_z is the deviation between the highest peaks to the lowest valley on the surface²⁵. This is calculated by:

$$R_z = R_p + R_v \quad (2)$$

where R_p is the height of the peak and R_v is the depth of the valley. Long range waviness was removed using a cutoff value of $\lambda_c = 0.025$ mm and was applied to all samples (unless noted).

Data availability

The authors declare that the data supporting the findings of this study are available within the paper and its Supplementary Information files. Should any raw data files be needed in another format they are available from the corresponding author upon reasonable request. Source data are provided with this paper.

Received: 9 February 2024; Accepted: 2 September 2024

Published online: 01 October 2024

References

- Goodall, R. H., Darras, L. P. & Purnell, M. A. Accuracy and precision of silicon based impression media for quantitative areal texture analysis. *Sci. Rep.* **5**, 10800. <https://doi.org/10.1038/srep10800> (2015).
- Chung, S., Im, Y., Kim, H., Jeong, H. & Dornfeld, D. A. Evaluation of micro-replication technology using silicone rubber molds and its applications. *Int. J. Mach. Tools Manuf.* **43**, 1337–1345. [https://doi.org/10.1016/S0890-6955\(03\)00164-0](https://doi.org/10.1016/S0890-6955(03)00164-0) (2003).
- Macdonald, D. A., Harman, R. & Evans, A. A. Replicating surface texture: Preliminary testing of molding compound accuracy for surface measurements. *J. Archaeol. Sci. Rep.* **18**, 839–846. <https://doi.org/10.1016/j.jasrep.2018.02.033> (2018).
- Nilsson, L. & Ohlsson, R. Accuracy of replica materials when measuring engineering surfaces. *Int. J. Mach. Tools Manuf.* **41**, 2139–2145. [https://doi.org/10.1016/S0890-6955\(01\)00080-3](https://doi.org/10.1016/S0890-6955(01)00080-3) (2001).
- Xu, C., Reece, C. & Kelley, M. Characterization of Nb SRF cavity materials by white light interferometry and replica techniques. *Appl. Surface Sci.* **274**, 15–21. <https://doi.org/10.1016/j.apsusc.2013.02.006> (2013).
- Bello, S. M., Vervenioutou, E., Cornish, L. & Parfitt, S. A. 3-dimensional microscope analysis of bone and tooth surface modifications: comparisons of fossil specimens and replicas. *Scanning* **33**, 316–324. <https://doi.org/10.1002/sca.20248> (2011).
- Nardin, P., Nita, D. & Mignot, J. Automation of a series of cutaneous topography measurements from silicon rubber replicas. *Skin Res. Technol.* **8**, 112–117. <https://doi.org/10.1034/j.1600-0846.2002.00309.x> (2002).
- Galbany, J. *et al.* Comparative analysis of dental enamel polyvinylsiloxane impression and polyurethane casting methods for SEM research. *Microsc. Res. Tech.* **69**, 246–252. <https://doi.org/10.1002/jemt.20296> (2006).
- Ge, M. *et al.* Routine characterization of 3D profiles of SRF cavity defects using replica techniques. *Supercond. Sci. Technol.* **24**, 035002. <https://doi.org/10.1088/0953-2048/24/3/035002> (2010).
- Rose, J. J. A replication technique for scanning electron microscopy: Applications for anthropologists. *Am. J. Phys. Anthropol.* **62**, 255–261. <https://doi.org/10.1002/ajpa.1330620305> (1983).
- Rosén, B. G., Blunt, L. & Thomas, T. R. On in-vivo skin topography metrology and replication techniques. *J. Phys. Confer. Ser.* **13**, 325–329. <https://doi.org/10.1088/1742-6596/13/1/076> (2005).
- Rodriguez, J. M., Curtis, R. V. & Bartlett, D. W. Surface roughness of impression materials and dental stones scanned by non-contacting laser profilometry. *Dent Mater* **25**, 500–505. <https://doi.org/10.1016/j.dental.2008.10.003> (2009).

13. Chee, W. W. L. & Donovan, T. E. Polyvinyl siloxane impression materials: A review of properties and techniques. *J. Prosthe Dent* **68**, 728–732. [https://doi.org/10.1016/0022-3913\(92\)90192-D](https://doi.org/10.1016/0022-3913(92)90192-D) (1992).
14. Pan, Y., Lin, C.-H., Wei, D. & Chen, C. Influence of surface roughness on particle deposition distribution around multi-slot cabin supply air nozzles of commercial airplanes. *Build Environ* **176**, 106870. <https://doi.org/10.1016/j.buildenv.2020.106870> (2020).
15. Zhu, D., Gillies, J. A., Etyemezian, V., Nikolich, G. & Shaw, W. J. Evaluation of the surface roughness effect on suspended particle deposition near unpaved roads. *Atmos. Environ* **122**, 541–551. <https://doi.org/10.1016/j.atmosenv.2015.10.009> (2015).
16. Yeh, C. P., Tsai, K. C. & Huang, J. Y. The effect of deposited dust on SCC and crevice corrosion of AISI 304L stainless steel in saline environment. *Materials (Basel)* <https://doi.org/10.3390/ma14226834> (2021).
17. Acharyya, S. G., Khandelwal, A., Kain, V., Kumar, A. & Samajdar, I. Surface working of 304L stainless steel: Impact on micro-structure, electrochemical behavior and SCC resistance. *Mater. Charact.* **72**, 68–76. <https://doi.org/10.1016/j.matchar.2012.07.008> (2012).
18. Montoya, T. *et al.* Influence of realistic, cyclic atmospheric cycles on the pitting corrosion of austenitic stainless steels. *J. Electrochem. Soc.* **170**, 041502. <https://doi.org/10.1149/1945-7111/acc42e> (2023).
19. Bryan, C. *et al.* FY21 Status Report: SNF Interim Storage Canister Corrosion and Surface Environment Investigations. Report No. M2SF-21SN010207056, 199 (Sandia National Laboratories, Albuquerque, NM, 2021).
20. Tanbakuchi, A. Photometrics Report: Cylinder Image Mapping. (Sandia National Laboratories, Albuquerque, New Mexico, 2021).
21. Knight, A., Schaller, R., Nation, B., Durbin, S. & Bryan, C. (Sandia National Laboratories, Albuquerque, New Mexico, 2022).
22. *Grit Size vs. Surface Roughness*, https://www.engineeringtoolbox.com/grit-size-surface-roughness-d_2096.html (2018).
23. Enos, D. & Bryan, C. Final report: Characterization of Canister Mockup Weld Residual Stresses. Report No. FCRD-UFD-2016-000064, 62 (U.S. DOE, 2016).
24. Novak, A. H. & Runje, B. in *7th Conference on Industrial Computed Tomography* (Leuven, Belgium, 2017).
25. Dashti, M. & Abdulaziz, A. A review on surface roughness (Ra) ranges for some finishing processes. *Int. J. Sci. Eng. Res.* **11** (2020).
26. Whitehorse, D. *Surfaces and Their Measurement* 1st edn, (Butterworth-Heinemann, 2004).

Acknowledgements

Sandia National Laboratories is a multimission laboratory managed and operated by National Technology and Engineering Solutions of Sandia LLC, a wholly owned subsidiary of Honeywell International Inc., for the U.S. Department of Energy's National Nuclear Security Administration under contract DE-NA-0003525. This article has been authored by an employee of National Technology & Engineering Solutions of Sandia, LLC under Contract No. DE-NA0003525 with the U.S. Department of Energy (DOE). The employee owns all right, title and interest in and to the article and is solely responsible for its contents. The United States Government retains and the publisher, by accepting the article for publication, acknowledges that the United States Government retains a non-exclusive, paid-up, irrevocable, world-wide license to publish or reproduce the published form of this article or allow others to do so, for United States Government purposes. The DOE will provide public access to these results of federally sponsored research in accordance with the DOE Public Access Plan <https://www.energy.gov/downloads/doe-public-access-plan>. This paper describes objective technical results and analysis. Any subjective views or opinions that might be expressed in the paper do not necessarily represent the views of the U.S. Department of Energy or the United States Government.

Author contributions

Nation and Knight wrote the manuscript and performed the experiments and analysis. Faubel and Ohlhausen performed the laser profilometry and Vice helped collect surface molds from the canister. Durbin and Bryan defined the scope of work and the research need. Durbin provided the spent nuclear fuel canister for surface evaluation. All authors edited and revised manuscript drafts.

Competing interests

The authors declare no competing interests.

Additional information

Supplementary Information The online version contains supplementary material available at <https://doi.org/10.1038/s41598-024-71992-1>.

Correspondence and requests for materials should be addressed to A.W.K.

Reprints and permissions information is available at www.nature.com/reprints.

Publisher's note Springer Nature remains neutral with regard to jurisdictional claims in published maps and institutional affiliations.

Open Access This article is licensed under a Creative Commons Attribution-NonCommercial-NoDerivatives 4.0 International License, which permits any non-commercial use, sharing, distribution and reproduction in any medium or format, as long as you give appropriate credit to the original author(s) and the source, provide a link to the Creative Commons licence, and indicate if you modified the licensed material. You do not have permission under this licence to share adapted material derived from this article or parts of it. The images or other third party material in this article are included in the article's Creative Commons licence, unless indicated otherwise in a credit line to the material. If material is not included in the article's Creative Commons licence and your intended use is not permitted by statutory regulation or exceeds the permitted use, you will need to obtain permission directly from the copyright holder. To view a copy of this licence, visit <http://creativecommons.org/licenses/by-nc-nd/4.0/>.

© The Author(s) 2024